

Elucidating the Roles of Nafion/Solvent Formulations in Copper-Catalyzed CO₂ Electrolysis

Pan Ding, Hongyu An, Philipp Zellner, Tianfu Guan, Jianyong Gao, Peter Müller-Buschbaum, Bert M. Weckhuysen,* Ward van der Stam, and Ian D. Sharp*



Cite This: *ACS Catal.* 2023, 13, 5336–5347



Read Online

ACCESS |

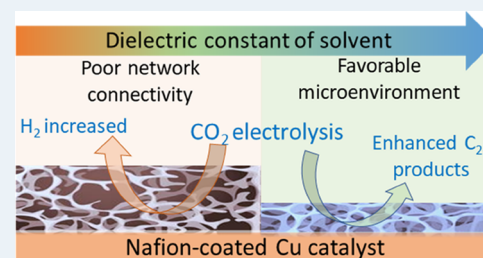
Metrics & More

Article Recommendations

Supporting Information

ABSTRACT: Nafion ionomer, composed of hydrophobic perfluorocarbon backbones and hydrophilic sulfonic acid side chains, is the most widely used additive for preparing catalyst layers (CLs) for electrochemical CO₂ reduction, but its impact on the performance of CO₂ electrolysis remains poorly understood. Here, we systematically investigate the role of the catalyst ink formulation on CO₂ electrolysis using commercial CuO nanoparticles as the model pre-catalyst. We find that the presence of Nafion is essential for achieving stable product distributions due to its ability to stabilize the catalyst morphology under reaction conditions. Moreover, the Nafion content and solvent composition (water/alcohol fraction) regulate the internal structure of Nafion coatings, as well as the catalyst morphology, thereby significantly impacting CO₂ electrolysis performance, resulting in variations of C₂₊ product Faradaic efficiency (FE) by >3×, with C₂₊ FE ranging from 17 to 54% on carbon paper substrates. Using a combination of ellipsometry and in situ Raman spectroscopy during CO₂ reduction, we find that such selectivity differences stem from changes to the local reaction microenvironment. In particular, the combination of high water/alcohol ratios and low Nafion fractions in the catalyst ink results in stable and favorable microenvironments, increasing the local CO₂/H₂O concentration ratio and promoting high CO surface coverage to facilitate C₂₊ production in long-term CO₂ electrolysis. Therefore, this work provides insights into the critical role of Nafion binders and underlines the importance of optimizing Nafion/solvent formulations as a means of enhancing the performance of electrochemical CO₂ reduction systems.

KEYWORDS: CO₂ reduction, nafion ionomer, catalyst ink formulations, Raman spectroscopy, Cu catalyst, reaction microenvironment



INTRODUCTION

The electrochemical CO₂ reduction reaction (CO₂RR), driven by renewable electricity, represents a promising approach to produce chemical feedstocks and fuels to enable the transition toward a carbon-neutral future.¹ Copper (Cu)-based catalysts have attracted increasing attention in the study of CO₂RR due to their unique ability to produce various multicarbon (C₂₊) products, such as ethylene (C₂H₄), ethanol (EtOH), and *n*-propanol (*n*-PrOH), which can be readily upgraded into commercial products through established industrial catalytic processes.^{1,2} While several CO₂RR catalysts can generate single-carbon (C₁) products (e.g., carbon monoxide and formate) with nearly 100% selectivity,^{3–7} selective conversion of CO₂ to multicarbon products on Cu-based catalysts remains challenging.⁸ Recently, numerous strategies have been reported to enhance the formation of C₂₊ products, while also suppressing the production of both C₁ products and the competing hydrogen evolution reaction (HER). These approaches mainly include structure and morphology engineering of Cu-based materials by surface modification,^{9–12} shape/size control,^{13,14} and alloying,^{15,16} as well as the regulation of reaction environments by adapting the electrolyte composition,^{17–19} means of gas transport,^{19,20} and types of ionomer

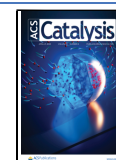
coatings.^{21–23} However, determining genuine limits to catalytic performance remains challenging since several factors beyond the nature of the catalyst itself can impact reaction outcomes. This is especially true for the case of catalytic nanomaterials, where different deposition methods, substrates, and ink formulations can influence key catalytic performance metrics, such as activity, stability, and selectivity. Understanding how these factors affect the electrochemical CO₂RR and leveraging these dependencies to engineer optimized systems is essential for further improving the performance of state-of-the-art catalyst materials.

Catalysts derived from nanoparticle suspensions are of particular interest due to their size- and shape-dependent properties, large surface-to-volume ratios, and compatibility with scaled manufacturing. This is reflected in CO₂RR research, where catalytic Cu nanoparticles and pre-catalytic

Received: October 23, 2022

Revised: March 14, 2023

Published: April 5, 2023



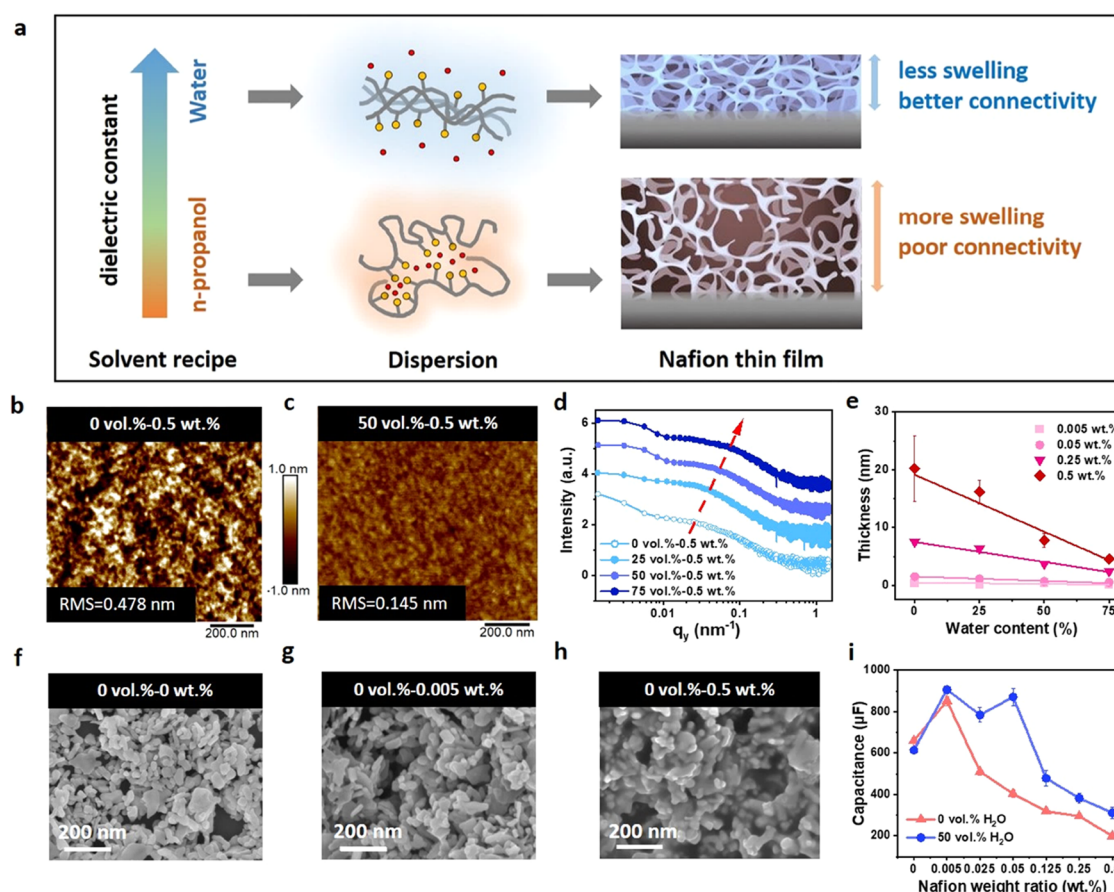


Figure 1. Structural and morphological analysis of Nafion films and catalyst layers. (a) Schematic illustration of the effects of Nafion/solvent formulations on the resulting Nafion films. (b, c) AFM images of Nafion spin-coated films on Si substrates produced from 0.5 wt % Nafion in solutions with 0 and 50 vol % water, respectively. (d) Horizontal line cuts of the 2D GISAXS data of Nafion films prepared with 0.5 wt % Nafion solutions with different water contents. (e) Thicknesses of spin-coated Nafion films on Si as a function of Nafion content and solvent composition, measured by spectroscopic ellipsometry. (f–h) SEM images of CuO nanoparticles on Si produced from solutions with 0 vol % water containing 0, 0.005, and 0.5 wt % Nafion, respectively. (i) Electric double-layer capacitance of CLs deposited on glassy carbon as a function of Nafion weight ratio and solvent composition, measured in Ar-purged 0.1 M K₂SO₄ aqueous electrolyte.

CuO_x nanoparticles have attracted considerable attention and have been shown to achieve high selectivity for C₂₊ products. In the typical approach to preparing cathodes for electrochemical CO₂ reduction, inks are first created by dispersing catalyst powders into water–alcohol solvent mixtures, after which they are deposited onto conductive substrates such as carbon paper. Ionomers are often added to these ink formulations to prevent agglomeration of nanoparticles, as well as to improve their adhesion to substrates. Nafion (perfluorosulfonic acid, PFSA) is the most widely used ionomer for electrode preparation in various electrochemical applications, including water splitting, oxygen reduction, and nitrogen reduction, as well as for carbon dioxide reduction.²⁴ Importantly, the dispersion of catalyst materials—especially nanoparticles—in solvent can be promoted by Nafion ionomers because they consist of hydrophobic PTFE chains and terminal hydrophilic sulfonic acid groups. Uniform deposition of catalyst with reduced aggregation on electrodes increases electrochemically active surface areas, thus ensuring high catalytic site loading and promoting the overall activity, while strong molecule–solid interactions enable Nafion to serve as a robust binder between the catalytic nanostructures and the support, thereby enhancing long-term operational stability.²⁵ Furthermore, the large proton conductivity of

Nafion, its hydrophobic/hydrophilic interactions, and mass transport characteristics can significantly affect the local environment in the vicinity of active sites.

It has been shown that different techniques for depositing particles dispersed in these inks can lead to variations in the structures of catalyst layers (CLs). For example, changes of thickness and porosity affect the mass transport and, thus, the reaction microenvironment under steady-state operation, thereby significantly influencing the selectivity for C₂₊ products.²⁶ In addition to the deposition approach, the catalyst ink formulation can also modify the structures and properties of resultant CLs, as well as the properties of Nafion at the catalyst surface. Indeed, previous studies have recognized that interactions between Nafion ionomers and different solvents can alter inner network connectivity/tortuosity, conductivity, and water uptake of resultant Nafion thin films, which enables regulation of the environment surrounding the catalyst.^{27–30} While it is expected that this can have a profound impact on the reaction microenvironment, systematic analyses of the role of ink formulations on CO₂RR performance characteristics are lacking and clear design rules for the optimization of activity, selectivity, and stability are required. Indeed, the ionomer/solvent formulations used in most studies are not rationally selected and vary considerably from one study to another. To

highlight this point, analysis of recent electrochemical CO₂RR literature reveals that the Nafion content in catalyst inks varies over a broad range, from 0 to 0.50 wt %, while the water content in water–alcohol solvent mixtures ranges from 0 to 80 vol.% (Table S3, and Figure S1). The pervasive inconsistency in Nafion content and solvent composition within catalytic ink formulations reflects the poor understanding of their effects on electrochemical CO₂RR. Consequently, analyses of catalytic function often neglect the critical role of Nafion in defining the reaction microenvironment and many reported catalysts risk being evaluated with nonoptimal Nafion/solvent formulations that underestimate the true performance characteristics of the underlying surface.

In this work, we systematically study the impact of Nafion/solvent formulations on Cu-catalyzed electrochemical CO₂RR. Using commercial CuO nanoparticles as the model pre-catalyst, we demonstrate that both the selectivity and stability of the resulting CLs are significantly affected by the Nafion/solvent formulation. In particular, we find that the presence of Nafion is crucial for the morphological stabilization of the electrodes, while the Nafion content and water–alcohol composition significantly impact the activity for multicarbon product formation. The presence of Nafion on the catalytic surface has a significant influence on the local reaction environment, where control of the CO₂ and H₂O reactants, as well as the CO intermediate, is essential for suppressing both HER and C₁ production, while promoting at the same time C–C coupling to form C₂₊ products.^{30,31} With this in mind, we correlate systematic electrochemical analyses of catalytic function with ex situ structural characterization and in situ Raman spectroscopic monitoring of CO₂RR on CLs to investigate the influence of Nafion/solvent formulations on activity, selectivity, and stability.

RESULTS AND DISCUSSION

As a starting point for understanding how ink formulations influence electrochemical CO₂RR, it is useful to first explore the roles of Nafion content and solvent composition on the structures and morphologies of deposited Nafion films and CLs. Previous studies of nanoscale Nafion films and microscale membranes have revealed that the dielectric constants of different solvents can alter the dispersion of Nafion ionomers in solution, which results in drastic structural changes of solution-derived Nafion films.^{25,27–29} As shown in Figure 1a, Nafion dispersions in low dielectric constant solvents (e.g., *n*-PrOH) lead to loose ionomer aggregates with linked sulfonic acid terminal groups. In contrast, high dielectric constant solvents (e.g., water) yield tightly packed aggregates with strong backbone interactions, resulting in improved inner network connectivity and reduced swelling upon Nafion film formation, as well as enhanced ionic conductivity and decreased water uptake.²⁸ Thus, we hypothesize that it should be possible to tune the structure of Nafion coatings surrounding catalyst layers by adjusting both the water/*n*-PrOH ratios and total Nafion content within catalyst ink formulations, thereby allowing controlled modification of key properties that can affect the CO₂RR, such as thickness, ionic conductivity, mass transport coefficients, and local micro-environments (e.g., pH, CO concentration, and CO₂/H₂O ratio).

To verify the expected dependence of deposited layer properties on ink formulations, we first examined pure Nafion films prepared by spin-coating solutions containing different

concentrations of Nafion and water. For this, formulations with seven Nafion weight fractions (0, 0.005, 0.025, 0.05, 0.125, 0.25, and 0.5 wt %) in water/*n*-PrOH solvent mixtures containing four water fractions (0, 25, 50, and 75 vol %) were investigated. These different compositions were selected to span the majority of ink compositions reported in the literature (Figure S1). As shown in a previous study, annealing of as-prepared Nafion films is able to lock-in the internal structural differences caused by the varying Nafion/solvent formulations.²⁸ Thus, we annealed all freshly prepared Nafion films and CLs at 80 °C prior to all measurements presented in this work.

Atomic force microscopy (AFM) images show representative surface morphologies of four dry Nafion films prepared from 0.5 wt % Nafion in solutions containing four different water fractions on polished Si substrates. All measured films were uniform, though the surface roughness was the largest for the case of absolute *n*-PrOH (0.48 nm) and decreased with increasing water content from 0.35 nm at 25 vol % to 0.13 nm at 75 vol % (Figures 1b,c and S2). Moreover, with increasing water content the porous structures within the film became smaller, as indicated by the three-dimensional (3D) AFM images in Figure S2 and in agreement with the expectation for higher network connectivity and smaller pore dimensions in films derived from higher-water-content solvents. This was also confirmed by grazing-incidence small-angle X-ray scattering (GISAXS) measurements of Nafion films since the horizontal line cuts revealed a shift of the *q_y* value of the domain structure from 0.025 to 0.075 nm^{−1} and, thus, a decreasing pore size as the water content was increased from 0 to 75 vol % (Figures 1d and S3). The smaller pore size and more densely packed structures are consistent with better inner connectivity and suggest higher proton conductivity of Nafion films derived from higher-water-content solvents.³²

The thicknesses of Nafion films as a function of solvent composition and ionomer content were quantified using spectroscopic ellipsometry (Figure 1e). Film thicknesses increased with increasing Nafion content: for the case of 0 vol % water (75 vol % water), the thickness increased from 0.3 to 20 nm (0.1–4.5 nm) as the Nafion content increased from 0.005 to 0.5 wt %. As indicated by these values, the Nafion film thickness decreased with increasing the water fraction. For example, the measured thickness of films prepared with 0.5 wt % Nafion decreased from 20 nm at 0 vol % water to 4.5 nm at 75 vol % water. These results indicate much thinner films with low Nafion and high water content, as well as a generally weaker dependence of thickness on the Nafion weight ratio with increasing water content.

Having characterized the influence of solvent and ionomer concentrations on resulting Nafion films, we then introduced catalytic particles to the ink formulations and investigated the properties of complete CLs. Commercial CuO nanoparticles were chosen as model pre-catalysts that can be reduced to catalytically active Cu under cathodic bias. Such nanoparticles offer high active site concentrations, along with the known superior catalytic activity of oxide-derived Cu compared with metallic Cu for generating C₂₊ products.^{33–35} Structural and morphological characterization revealed the particles to comprise the pure monoclinic phase of CuO (JCPDS No. 80-1268), with an average size of ~50 nm (Figures 1f–h and S4). After adding Nafion ionomer into catalyst inks, no significant changes to the X-ray diffraction (XRD) data were observed (Figure S4). However, scanning electron microscopy

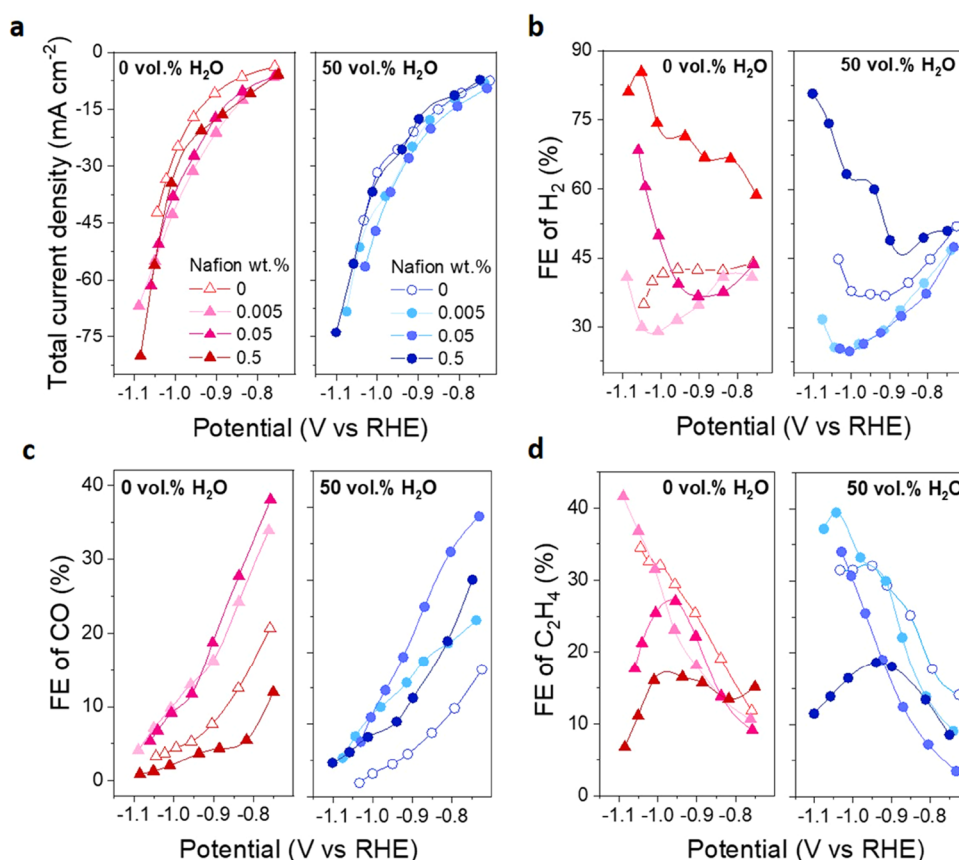


Figure 2. Effect of Nafion/solvent formulations on potential-dependent CO_2 electrolysis. Catalytic performance of electrodes prepared by different Nafion/solvent formulations evaluated in terms of total current density (a), as well as Faradaic efficiency of H_2 (b), CO (c), and C_2H_4 (d).

(SEM) images showed clear indications for the presence of Nafion coatings on CLs deposited from 0.5 wt % Nafion solutions (Figure 1h). Notably, X-ray photoelectron spectroscopy (XPS) revealed increasing attenuation of the Cu 2p signals with increasing Nafion content. No chemical changes were observed within the Cu 2p core level region, indicating that the CuO is preserved upon contact with Nafion. However, for the highest Nafion content of 0.5 wt %, photoemission from the catalyst particles was nearly completely suppressed (Figure S5). Given the XPS sampling depth through organic material is on the order of ~ 10 nm,³⁶ these findings indicate that formulations of higher Nafion weight ratio yield increasing thicknesses of Nafion atop CuO particles at the nm scale. Consistent with this conclusion, C 1s photoemission intensities associated with the C–F₂ and C–O bonding in Nafion increase with increasing Nafion content.

Transmission electron microscopy (TEM) was performed to verify the presence of Nafion on catalyst particles, as well as the qualitative dependence of film thickness on solvent composition. In particular, TEM images from CuO nanoparticles deposited from solutions containing 0.5 wt % Nafion and various water/*n*-PrOH solvent ratios were acquired. Consistent with the spectroscopic ellipsometry data described above, Nafion coatings were observed around CuO nanoparticles for all samples and the thickness of Nafion coatings was reduced with increasing water content (Figure S6). The consistent trend of decreasing film thickness with increasing water content indicates that the impact of formulations on deposited Nafion coatings persists when CuO nanoparticles are introduced to form catalyst inks.

As a basis for understanding the influence of Nafion at the surfaces of CuO particles on CO_2 RR activity and selectivity, we evaluated the electrochemically active surface areas (ECSAs) by measuring the double-layer capacitances of drop-casted CLs on glassy carbon substrates in 0.1 M K_2SO_4 aqueous electrolyte (Figure 1i). SEM images revealed that CLs formed without Nafion contained many large agglomerates, while the addition of Nafion and its increasing weight ratio in the catalyst ink significantly improved the homogeneity and dispersity of CuO nanoparticles (Figure S7). Accordingly, compared to layers prepared in the absence of Nafion, the measured double-layer capacitances increased and peaked at the lowest Nafion weight fraction of 0.005 wt %. These findings indicate that suitably low Nafion content can be beneficial for creating higher loadings of active sites by improving the dispersion of catalyst nanoparticles. However, the peaked dependence suggests that higher Nafion content results in the blocking of active sites due to the formation of thick coatings over the nanoparticle surfaces. For layers prepared with 50 vol % water, large double-layer capacitances were preserved over a broader range of Nafion wt % (up to ~ 0.05 wt %) and these values were also larger for all Nafion contents compared to those prepared with 0 vol % water, which is consistent with the observed reduction of Nafion thicknesses with increasing water content.

In summary, we conclude that Nafion ionomer is required to ensure homogeneous dispersion of CuO pre-catalysts. The properties of Nafion coatings can be modified by tuning both Nafion and water/alcohol content in ink formulations. Specifically, increasing Nafion content leads to thicker Nafion coatings that can block active sites of CLs and decrease

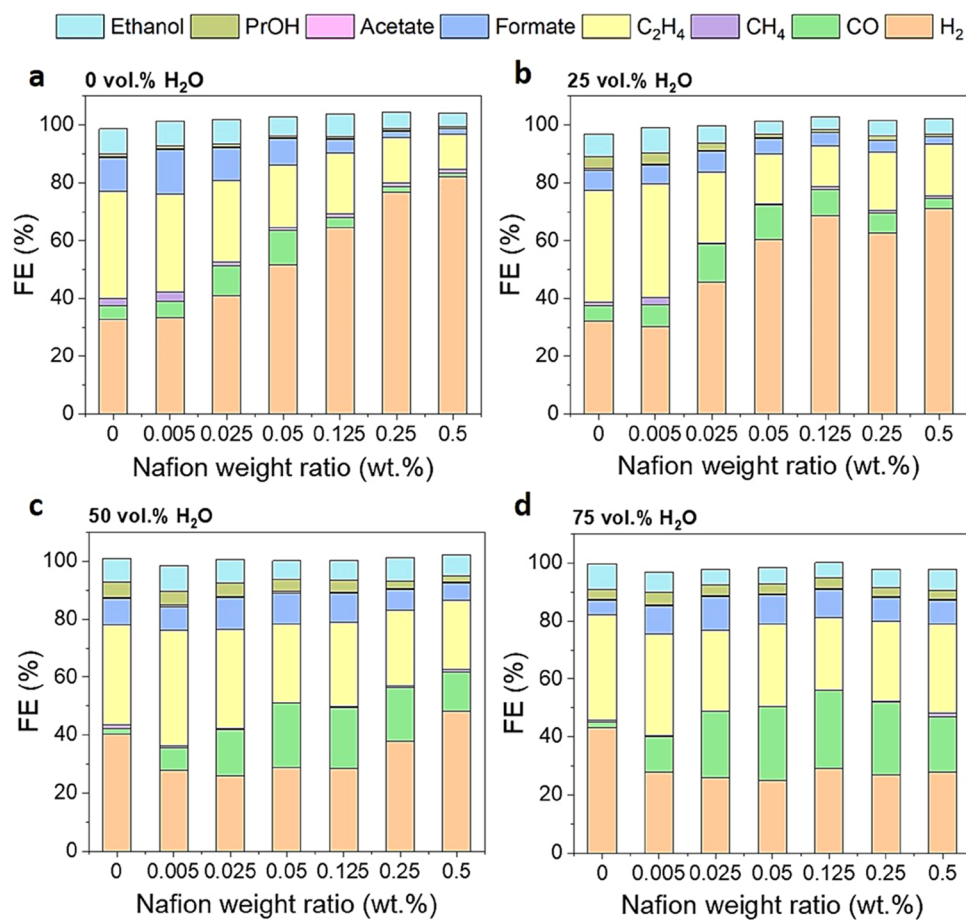


Figure 3. Product distributions from CLs during chronopotentiometric CO_2 electrolysis at a total current density of -50.0 mA cm^{-2} . The electrodes were prepared by varied Nafion/solvent formulations containing seven different Nafion weight ratios (0, 0.005, 0.025, 0.05, 0.125, 0.25, and 0.5 wt %) and four different water contents, namely, (a) 0, (b) 25, (c) 50, and (d) 75 vol %.

catalytic surface areas, which can be balanced by increasing the water content (i.e., decreasing alcohol content) to improve the inner structure of Nafion coatings. Furthermore, when subject to CO_2 electrolysis, Nafion coatings possessing different thicknesses and inner network connectivities are likely to significantly impact the reaction microenvironment and, thus, reaction selectivities. Therefore, it is expected that the incorporation of Nafion can promote the activity of CLs for electrochemical CO_2RR , but that an optimum catalyst ink formulation exists to balance these competing properties.

The impact of Nafion/solvent formulations on electrochemical CO_2RR was investigated using electrodes based on carbon paper substrates in a conventional H-cell under 0.5 M KHCO_3 with continuous CO_2 bubbling and a constant catalyst mass loading of 0.5 mg cm^{-2} . Gas products of CO_2 electrolysis, including H_2 , CO , CH_4 , and C_2H_4 , were analyzed at seven different potentials (Figure 2). Importantly, electrodes prepared without Nafion exhibited the lowest total current densities (Figure 2a), which is consistent with agglomeration and restructuring of weakly bound catalytic particles. Although the current density vs potential (J - E) characteristics from all electrodes prepared with Nafion were similar, those prepared with 50 vol % water content displayed slightly higher total current densities across the entire potential range compared to those prepared without water (for clarity, these data are also provided in merged plots in Figure S8a). This result agrees with the reduced Nafion thickness, improved inner network

connectivity, and higher ESCA for these CLs. Nevertheless, the weak dependence of the total current density on catalyst ink formulation implies that ionic transport limitations do not play a dominant role for the Nafion thickness regime investigated here, which is consistent with the findings of Kim et al.²³

Corresponding gas chromatography (GC) measurements reveal the strong influence of the catalyst ink formulation on the product yield. In particular, we observe significant suppression of HER with the inclusion of low Nafion weight fractions. For ink formulations containing 50 vol % water, similar HER suppression is obtained with both 0.005 and 0.05 wt % Nafion, with an absolute minimum H_2 FE of 24.5% at $-1.00 \text{ V}_{\text{RHE}}$ for the electrode produced from 50 vol % water and 0.05 wt % Nafion (Figure 2b). For those electrodes produced in the absence of water, the H_2 FE is consistently larger and rapidly increases with increasing Nafion content. At the highest Nafion content of 0.5 wt %, vigorous hydrogen generation with maximum H_2 FEs in excess of 80% was observed, though the H_2 FEs remained lower across the entire potential range for the 50 vol % water compared to the 0 vol % water samples. In addition, the production of CO was promoted and the yield of CH_4 was slightly reduced for all Nafion contents at 50 vol % water relative to those at 0 vol % (Figures 2c and S8c–f). As a result, the production of C_2H_4 was enhanced at 50 vol % water, especially in the region of low Nafion weight ratio where HER was significantly suppressed. The maximum C_2H_4 FE values of >40% were achieved at

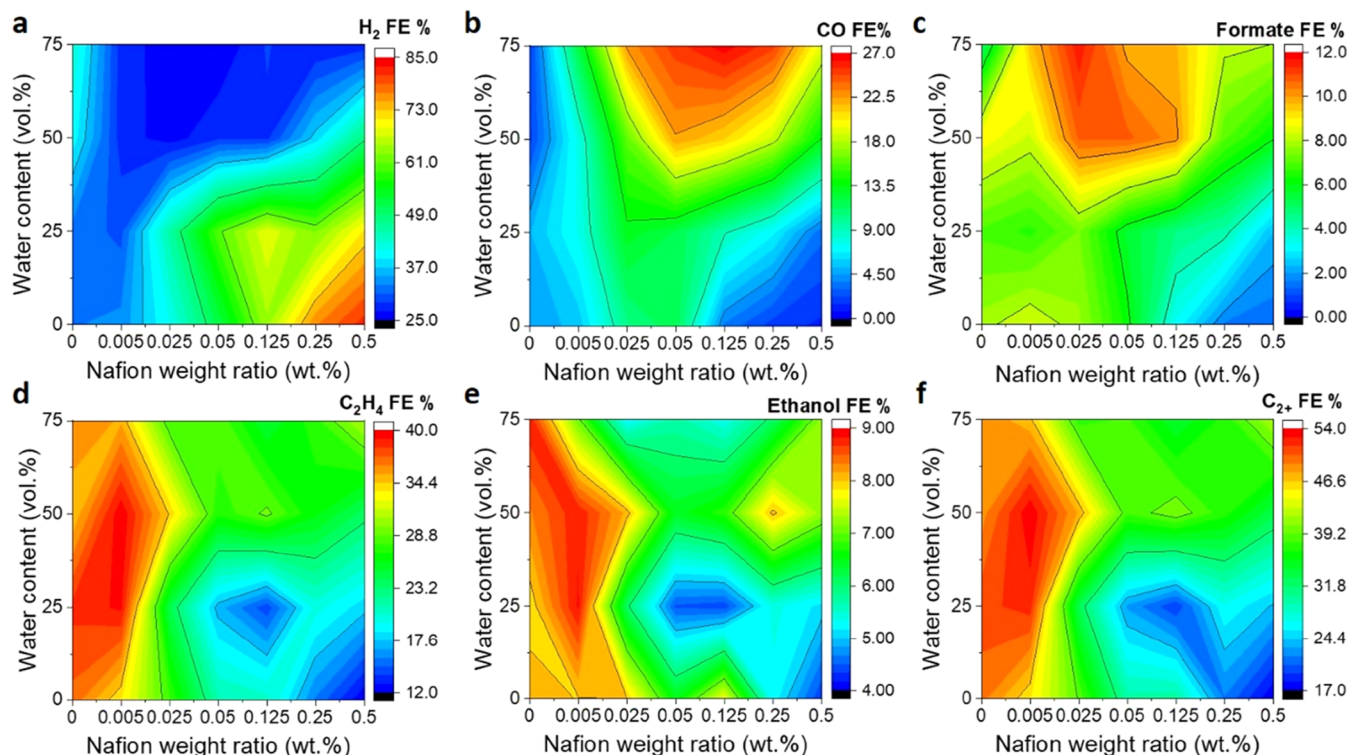


Figure 4. Effect of Nafion/solvent formulations on the selectivity of chronopotentiometric CO_2 electrolysis at a total current density of -50.0 mA cm^{-2} on carbon paper. Heatmaps of Faradaic efficiency for H_2 (a), CO (b), formate (c), C_2H_4 (d), ethanol (e), and C_{2+} products (f).

0.005 wt % regardless of initial water content (Figure 2d), while the one prepared from the ink of 50 vol % water demonstrated superior C_2H_4 FEs across the whole potential range compared to the one prepared from the ink without water (Figure S8g). Such performance is comparable with that measured on previously reported oxide-derived Cu catalysts.³⁷ The C_2H_4 FEs were generally reduced with increasing Nafion content, with those prepared with 0.5 wt % Nafion remaining below 20% at all potentials. Accordingly, the partial current density of C_2H_4 decreased by a factor of approximately $3.6\times$ near $-1.1 \text{ V}_{\text{RHE}}$ from -27 mA cm^{-2} at 0.005 wt % Nafion to less than -8 mA cm^{-2} at 0.5 wt % Nafion for both water contents (Figure S8h). Here, it is important to note that electrodes prepared without Nafion exhibited reasonably large C_2H_4 FEs in excess of 30%. However, these electrodes were characterized by poor stabilities compared to those containing Nafion, as discussed below.

To evaluate the impact of Nafion/solvent formulations on complete product distributions during long-term CO_2 electrolysis under optimal conditions, as well as to assess CL stabilities, we performed chronopotentiometry tests on all samples for a duration of 5 h and analyzed both gas and liquid products (Figure 3). These experiments were performed at a constant current of -50 mA cm^{-2} , which was selected to correspond to the conditions that promote highest CO_2RR and lowest HER Faradaic efficiency (as discussed above and shown in Figure 2). In total, 17 different products of CO_2RR were detected using GC and nuclear magnetic resonance spectroscopy (^1H NMR), in agreement with previous studies,² but only the 8 major products (hydrogen, carbon monoxide, methane, ethylene, formate, acetate, *n*-propanol, and ethanol) were quantified (Figures S9 and S10). The average FEs for these products during the 5 h of CO_2 electrolysis as a function of

Nafion weight ratio and solvent composition in the ink formulation are plotted in Figure 3a–d and confirm the strong dependence of product distribution on both Nafion content and solvent composition. Here, it is noted that the observed FEs are not identical to those reported near 50 mA cm^{-2} in Figure 2 since certain formulations yielded unstable performance during the long-term evaluation. In general, the consequence of these instabilities was to increase HER at the cost of CO_2RR activity (see below).

For all electrodes, the major products comprised C_2H_4 , CO, and H_2 . To specifically analyze the selectivity changes, the average FE of five dominant products at different Nafion/solvent formulations is compared in heatmaps (Figure 4a–e), along with a heatmap for the total FE for C_{2+} products (Figure 4f). Corresponding heatmaps for minor products are available in Figure S11. From these data, several distinct regions can be identified. First, HER is effectively suppressed over an extended region spanning low Nafion and/or high water content, where the H_2 FEs were all below 30% (top left of heatmaps). Notably, the H_2 FEs at each Nafion weight ratio, particularly high Nafion weight ratio ($>0.05 \text{ wt } \%$), were continuously reduced with a gradual increase of water content in ink formulations. For instance, for electrodes prepared with 0.5 wt % Nafion, the H_2 FE was drastically reduced from 80% at 0 vol % water to 28% at 75 vol % (Figure 4a). Consistent with the results discussed above, more vigorous H_2 production was associated with CLs prepared with high Nafion and low water content (bottom right of heatmaps). Within the region of suppressed HER, C_{2+} products were dominant for all CLs prepared with low Nafion content, regardless of water fraction. While C_2H_4 was the primary product, FEs for both EtOH and *n*-PrOH increased with increasing water content for CLs prepared with low Nafion content (Figures 4e and S11h). That

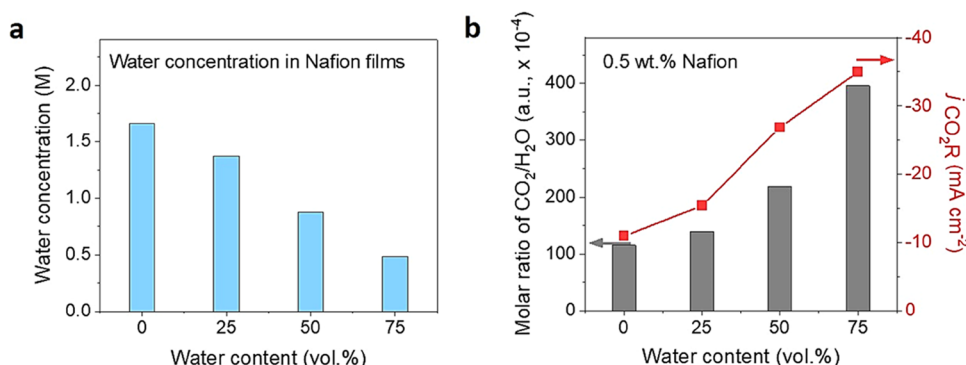


Figure 5. Effect of solvent composition on water uptake and reaction microenvironment during CO₂ electrolysis. (a) Plots of calculated water concentration in Nafion films from in situ ellipsometry tests vs water content in Nafion solutions. (b) Estimation of molar ratio of CO₂/H₂O (gray bars) on the basis of measured water concentration within Nafion coatings in (a) and the corresponding partial current densities for CO₂R (red squares) in chronopotentiometry test of -50 mA cm^{-2} .

is to say, CLs prepared at high water content and low Nafion content appear to enhance the adsorption of not only CO intermediate for C–C coupling but also key C₂ intermediates for subsequent C₁–C₂ coupling. Taken together, the dependence of these products on ink formulation resulted in a similar form of the heatmap for the total FE of C₂₊ products varying from a peak value of 54% at low Nafion content to a minimum of 17% for high Nafion and low water content (Figure 3f).

Interestingly, the production of CO was drastically affected by Nafion/solvent formulations with CO FE ranging from 0 to ~27.0%. In particular, CO production was especially favored for formulations possessing both high water and high Nafion content (Figure 4b). In addition, the FE of another major C₁ product, namely, formate, increased in the CO-favored region (Figure 4c), though its peak FE occurred at slightly lower Nafion content. At high water content, this direct competition between C₁ and C₂₊ products suggests enhanced activity for C₂₊ products at low Nafion content that is disturbed at a higher Nafion content.

The complete set of observations presented above suggests a basis for understanding CL performance characteristics in terms of the evaluated properties of Nafion as a function of ink composition. As a starting point, we first considered the role of Nafion in impeding CO₂ transport to the Cu surface. As described in Supporting Note 1 in the Supporting Information, for all chronopotentiometric measurements reported here, partial current densities for CO₂R (*j*_{CO₂R}) were sufficiently small to ensure that the diffusive flux of CO₂ to the surface exceeds the flux associated with CO₂ consumption via CO₂R. Thus, for the range of Nafion thicknesses investigated here, the system is governed by surface reaction rate kinetics rather than mass transport of CO₂. While this conclusion may be surprising in light of the strong dependence of CO₂R selectivity and product distribution on the catalyst ink formulation, it is important to recognize that the internal structure and network connectivity of Nafion coatings are significantly impacted by the solvent composition, as described above. In particular, improved internal network connectivity, which is promoted by high water/alcohol fractions within the solvent, is expected to reduce water uptake within the formed Nafion layers, which could significantly modify the relative availability and accumulation of reactants and intermediates at Cu catalyst surfaces.

To test this hypothesis and understand the impact of different ink formulations on the reaction microenvironment,

we have estimated the local molar concentration ratio of CO₂ and H₂O ([CO₂]/[H₂O]) on the basis of measured water concentration in Nafion films using in situ ellipsometry and corresponding CO₂R partial current densities in chronopotentiometry tests (Figure 5). For a fixed Nafion weight fraction of 0.5 wt %, increasing water content in the solvent solution resulted in smaller swelling fractions of Nafion films during subsequent exposure to humidified environments (Table S1). This finding is consistent with the scheme in Figure 1a and indicates decreasing water uptake (i.e., decreasing concentration of water molecules compared to the concentration of Nafion SO₃[−]) when treated with water-saturated N₂ (Figure 5a). Combined with the partial current densities for all CO₂R products in 5 h of chronopotentiometry electrolysis, this water concentration reveals a substantial increase of the calculated molar ratio [CO₂]/[H₂O] with increasing water content. In particular, when operated at a total current density of -50 mA cm^{-2} the molar ratio [CO₂]/[H₂O] increased by 3.4× for the films prepared with 75 vol % water compared to those prepared with 0 vol % water. This important change to the reaction microenvironment corresponds to an enhanced CO₂R activity, with partial current density *j*_{CO₂R} increasing from -10.9 mA cm^{-2} at 0 vol % to -35.0 mA cm^{-2} at 75 vol % (Figure 5b). Together with our insights from the structural analysis of Nafion films in Figure 1, we can thus conclude that this dramatically higher molar ratio [CO₂]/[H₂O] arises from the formation of thinner and denser Nafion coatings with better inner network connectivity, resulting in enhanced CO₂ availability near the copper surface for ink formulations comprising higher water content. This finding is also consistent with the observed product distribution, which favors CO₂R over HER. In addition, the decreased water concentration in the reaction environment could have a significant impact on the local pH. While this quantity is extremely difficult to quantify, it is important to recognize that one OH[−] ion is generated for each e[−] consumed by CO₂R.³⁸ Thus, suppressed water uptake in Nafion films could promote more alkaline environments that favor C–C coupling reactions.

To further explore the underlying mechanisms of the observed reactivity differences, we monitored the structural evolution of Cu catalysts and their local microenvironments with the help of ex situ SEM and in situ Raman spectroscopy measurements. First, six representative carbon paper-based electrodes, including those prepared with 0 and 50 vol % water combined with 0, 0.005, and 0.5 wt % Nafion, were

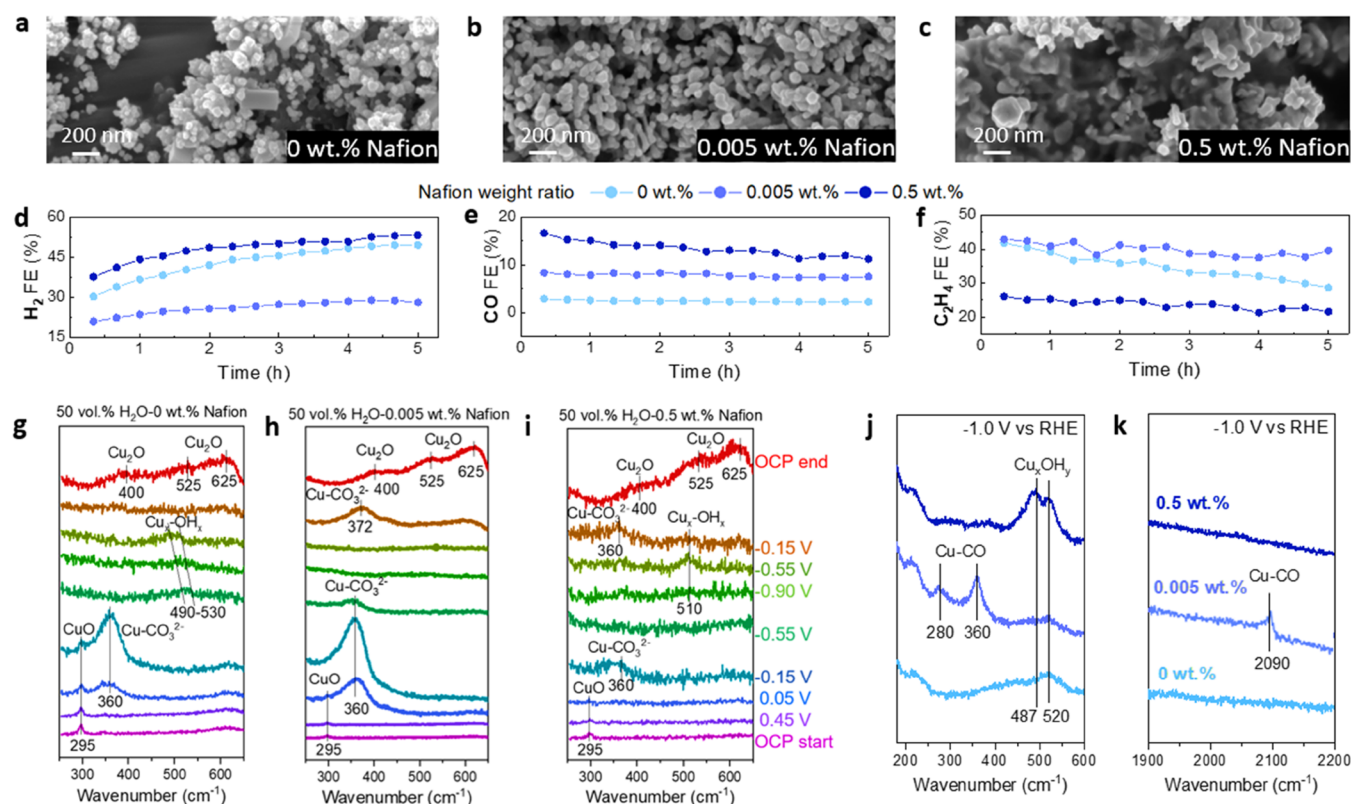


Figure 6. Effect of Nafion weight ratio on morphological and compositional changes of CLs, as well as local reaction environments, during long-term CO₂ electrolysis. (a–c) SEM images of three carbon paper-based electrodes after 5 h of CO₂ 5 h of chronopotentiometry test at -50 mA cm^{-2} : 50 vol % water-0 wt % Nafion (a), 50 vol % water-0.005 wt % Nafion (b), and 50 vol % water-0.5 wt % Nafion (c). Changes of Faradaic efficiencies of H₂ (c), CO (d), and C₂H₄ (e) within 5 h of CO₂ electrolysis on three electrodes. (g–k) In situ Raman spectra recorded in cyclic voltammetry tests (g–i) and chronoamperometry tests (j, k) on three electrodes.

characterized during 5 h chronopotentiometry tests at a fixed total current density of -50 mA cm^{-2} .

The morphology after CO₂ electrolysis was investigated by SEM, as shown in Figures 6a–c and S12a–c. Direct comparison of selected catalyst layers before and after operation is provided in Figures S13 and S14. Notably, large cubic Cu crystals with size of 250–600 nm were observed on the electrode without Nafion, which suggested that significant Cu reconstruction occurred during CO₂ electrolysis. Such reconstruction would not only reduce the electrochemically active surface area but can also cause a change of selectivity due to variation of crystal facets between the in situ grown Cu cubes and pristine CuO-derived Cu nanoparticles.^{39,40} Moreover, a decrease of surface coverage of Cu and exposure of the bare carbon paper substrate, indicated possible detachment of Cu nanoparticles. Such morphological instabilities are consistent with prior investigations of Cu-based CO₂R electrocatalysts, which are susceptible to aggregation, delamination, dissolution–redeposition, and facet evolutions under reaction conditions.^{2,41} These severe morphological changes likely account for increasing H₂ FE from 30 to 50% during the 5 h chronoamperometric experiment (Figure 6d). In contrast, the morphologies and coverages of CLs containing Nafion were effectively preserved, suggesting that the ionomer serves as an effective binder and encapsulant to enhance adhesion and confine particles, thereby reducing the surface mobility, detachment, and dissolution/redeposition processes that characterize bare Cu electrocatalysts. Therefore, Nafion ionomer was necessarily required to ensure the structural

stability of Cu in CO₂ electrolysis. However, thicker Nafion coatings obtained from inks containing higher Nafion weight ratios (0.5 wt %) lead to reduced electrochemically active surface areas, blocking of active sites, and enhanced HER.

To gain insight into the local microenvironments near the Cu catalyst surfaces, we monitored the oxidation state of Cu (Cu₂O and/or CuO) and the presence of various adsorbed intermediates and ions during electrochemical CO₂RR measurements using in situ Raman spectroscopy (Figures 6g–k and S12). As a basis for these experiments, we first analyzed the catalyst activation process by cyclic voltammetry (CV) in the pre-catalytic region between the open circuit potential (OCP) and $-0.9 \text{ V}_{\text{RHE}}$, during which the first CV sweep always showed a distinct reduction wave for conversion of CuO to metallic Cu (Figure S15). Accordingly, on all six samples, we observed the characteristic peak for CuO at $\sim 295 \text{ cm}^{-1}$ at OCP, which disappeared when the applied potential was more cathodic than $-0.15 \text{ V}_{\text{RHE}}$, suggesting that CuO can be readily reduced to catalytically active Cu. In addition, a broad band at $\sim 360 \text{ cm}^{-1}$ emerges starting at $0.05 \text{ V}_{\text{RHE}}$ and persists until $-0.15 \text{ V}_{\text{RHE}}$. Recent reports have assigned this band to surface-adsorbed bidentate carbonate species (Cu–CO₃²⁻) associated with the CuO reduction process in the presence of KHCO₃ electrolyte and hydroxyl species.^{42–45} It is important to note that this mode is similar in energy to the linear Cu–C stretch (from adsorbed *CO on Cu) that could be indicative of adsorbed *CO, a key intermediate in C₂+ product formation. However, this can be excluded due to the absence of the spectral signature of Cu–CO rotational modes

at 280 cm^{-1} , the corresponding broad linewidth of the 360 cm^{-1} vibrational feature, and its presence in the pre-catalytic potential range associated with CuO to Cu activation. Thus, the 360 cm^{-1} mode observed between 0.05 and $-0.15\text{ V}_{\text{RHE}}$ is assigned to bidentate $\text{Cu}-\text{CO}_3^{2-}$, and disappears upon complete activation of the catalyst to Cu, in line with recent in situ Raman spectroscopy investigations on the dynamics of CO_2 to CO activation in this potential regime.⁴⁵

When scanning to more cathodic potentials from -0.55 and $-0.90\text{ V}_{\text{RHE}}$ and then scanning back to $-0.15\text{ V}_{\text{RHE}}$, multiple broad peaks in the range of ~ 490 to $\sim 530\text{ cm}^{-1}$ arise, particularly on the electrodes fabricated without Nafion and with 0.5 wt % Nafion (Figure 6g–i).^{43,46,47} These spectral features around 500 cm^{-1} have been heavily debated in the literature: some works show evidence for the presence of hydroxide ions due to severe HER,⁴⁸ whereas others including our own have used isotope labeling to show that bands in this regime correspond to carbon-containing reaction intermediates.^{44,45} A definite assignment of the bands in this region remains challenging due to the low signal-to-noise ratio, but the presence of Cu_x-OH_y is inferred due to the likely consumption of protons during HER (Figure 2b). As shown in Figure 6d, HER dominates for 0 and 0.5 wt % Nafion, in line with the presence of vibrational features around 500 cm^{-1} (Figure 6g). For the case of electrodes prepared with 0.005 wt % Nafion, peaks around 500 cm^{-1} were extremely weak, in agreement with suppressed HER (Figure 6d,h). In general, electrodes prepared with high Nafion content (0.5 wt %) exhibited much weaker $\text{Cu}-\text{CO}_3^{2-}$ and/or potential Cu_x-OH_y Raman scattering intensities than those prepared without Nafion or with low Nafion content (0.005 wt %). This could be a consequence of the reduced ECSA and limited carbonate content near the surface during the Cu_2O -to-Cu reduction process in the case of thicker Nafion coatings at 0.5 wt %. Finally, on all six electrodes, Cu at the surface was partially re-oxidized into Cu_2O when the CV concluded at OCP due to inevitable exposure of the electrode to the aqueous electrolyte, as indicated by three corresponding peaks at around 400, 525, and 625 cm^{-1} assigned to Cu_2O (Figure 6g–i).^{42,43}

Immediately after the activation process, we continued with chronoamperometry tests at a fixed potential of -1.0 V on all electrodes and simultaneously analyzed the local microenvironment by in situ Raman spectroscopy (Figures 6j,k, S12j,k, and S16). Prior to the application of potential, all electrodes exhibited two peaks near 525 and 625 cm^{-1} at OCP, which are attributed to the re-oxidized Cu_2O described above (Figure S17). Upon application of $-1.0\text{ V}_{\text{RHE}}$ and the associated onset of CO_2 electrolysis, Cu_2O was reduced to metallic Cu and the corresponding peaks for Cu_2O completely vanished. The specific Raman bands from the carbon paper substrates were observed on all electrodes, with peaks at around 1315 and 1600 cm^{-1} . Remarkably, on the electrode with 50 vol % water and 0.005 wt % Nafion, the sharp peak at 360 cm^{-1} ($\text{Cu}-\text{C}$ linear stretching mode from adsorbed $^*\text{CO}$ on Cu) accompanied by two additional peaks at 280 ($\text{Cu}-\text{CO}$ rotation) and 2090 cm^{-1} (linear CO stretching mode) provide a direct indication for the presence of surface-adsorbed CO ($\text{Cu}-\text{CO}$). More importantly, the peak intensity at 360 cm^{-1} was much higher than that at 280 cm^{-1} , which is consistent with a high CO surface coverage that is beneficial for C–C coupling to produce C_{2+} products.^{42,49} As a result, only the electrode with 50 vol % water and 0.005 wt % Nafion demonstrated moderate CO FE of $\sim 7.5\%$ and the highest

C_2H_4 FE of $\sim 40\%$ throughout 5 h of electrolysis and also the highest C_{2+} FE of $\sim 54\%$ among all six carbon paper-based electrodes (Figure 6e,f), in agreement with the in situ Raman spectroscopy data. In contrast, those characteristic peaks for $\text{Cu}-\text{CO}$ were not detected on electrodes without Nafion or with a high Nafion weight ratio (0.5 wt %). Instead, carbonate bands at $360\text{ (Cu}-\text{CO}_3^{2-})$ and 1067 cm^{-1} (CO_3^{2-} symmetric stretching mode) and peaks between 480 and 610 cm^{-1} were observed,⁴² particularly on the electrodes with 0.5 wt % Nafion (Figure S16). On Cu surfaces, high coverage of carbonates and hydroxides rather than high coverage of CO is inevitably associated with strong HER and reduced C_{2+} production. Correspondingly, electrodes without Nafion suffered from increasing H_2 FE from $\sim 20\%$ to $>45\%$ and decreasing C_2H_4 FE from ~ 40 to $\sim 30\%$ over 5 h. Electrodes with 0.5 wt % Nafion performed even worse, constantly possessing the highest H_2 FE and the lowest C_2H_4 FE within 5 h (Figures 6d,f and S12d,f). Interestingly, the electrode with 0 vol % water and 0.005 wt % Nafion also presented high C_2H_4 FE of $\sim 40\%$ and low H_2 FE of $\sim 20\%$ at the beginning of the experiment, but the production of CO and C_2H_4 continuously decreased and HER increased over 5 h. Taken together, these findings reveal that only the combination of high water/alcohol fraction and low Nafion weight ratio in the solvent ink is able to provide a stable and favorable microenvironment with high CO surface coverage to facilitate C_{2+} production in long-term CO_2 electrolysis. Future work, devoted to in situ probing of local reaction environment, surface adsorbate coverages, and catalyst oxidation state via correlative X-ray and vibrational spectroscopies could provide even further insights into the important role of ionomer coatings on CO_2RR activity and selectivity.

CONCLUSIONS

In this work, we systematically studied the impact of Nafion/solvent formulations on CO_2 electrolysis using CuO as a model catalyst. Using high-surface-area carbon paper supports, the performance of electrochemical CO_2RR in terms of activity, selectivity, and stability was significantly influenced by varying Nafion/solvent formulation. Combining structural and morphological characterization of Nafion films and CLs with in situ spectroscopic analysis of the local microenvironment enabled specific insights into the role of Nafion on reaction outcomes. In particular, the impact of Nafion/solvent formulation on CO_2 electrolysis originates from three major aspects: the evolution of catalyst structure, modulation of local microenvironment, and accumulation of surface adsorbates. Specifically, morphological restructuring and delamination of weakly bound catalysts were effectively suppressed by the addition of Nafion into the catalyst ink, resulting in stabilized product distributions. Furthermore, tuning both the thickness of Nafion coatings and their inner network connectivity by changing both the Nafion and water content in the catalyst ink formulations impacted the local concentrations of CO_2 and H_2O in the reaction microenvironment and the CO surface coverage, as evidenced by in situ Raman spectroscopy. Use of high water content of 50–75 vol % in catalyst inks is recommended to optimize the quality of Nafion coatings for improved CO_2RR performance. Although this study addresses aqueous H-cell type reactor configurations, it is reasonable to expect that the strong dependence of ink formulations on catalyst performance characteristics will also be observed for other cell types, such as those comprising gas diffusion electrodes (GDEs). While morphological stabilization by

Nafion is likely to also play an important role in such systems, the higher operating current densities afforded by improved mass transport at the three-phase interface, as well as their operation under highly alkaline conditions, suggest that optimal Nafion thicknesses and internal structures will differ from those reported here, thus motivating analogous studies for GDEs electrodes in the future. Overall, these findings provide a scientific basis for understanding and designing Nafion/solvent formulations for manufacturing electrodes in CO₂ electrolysis, and motivate further innovation in catalyst ink formulation development, including the use of novel ionomers and solvents specifically tailored for the desired electrochemical application.

■ ASSOCIATED CONTENT

SI Supporting Information

The Supporting Information is available free of charge at <https://pubs.acs.org/doi/10.1021/acscatal.2c05235>.

Preparation of Nafion films and working electrodes; basic characterization of samples; spectroscopic ellipsometry; in situ Raman spectroscopy experiments; and electrochemical CO₂RR testing (PDF)

■ AUTHOR INFORMATION

Corresponding Authors

Bert M. Weckhuysen – *Inorganic Chemistry and Catalysis, Department of Chemistry, Utrecht University, 3584 CG Utrecht, The Netherlands*; orcid.org/0000-0001-5245-1426; Email: b.m.weckhuysen@uu.nl

Ian D. Sharp – *Walter Schottky Institute and Physics Department, Technical University of Munich, 85748 Garching, Germany*; orcid.org/0000-0001-5238-7487; Email: sharp@wsi.tum.de

Authors

Pan Ding – *Walter Schottky Institute and Physics Department, Technical University of Munich, 85748 Garching, Germany*

Hongyu An – *Inorganic Chemistry and Catalysis, Department of Chemistry, Utrecht University, 3584 CG Utrecht, The Netherlands*; orcid.org/0000-0003-4646-9819

Philipp Zellner – *Walter Schottky Institute and Physics Department, Technical University of Munich, 85748 Garching, Germany*

Tianfu Guan – *Chair for Functional Materials, TUM School of Natural Sciences, Technical University of Munich, 85748 Garching, Germany*; orcid.org/0000-0002-9887-9265

Jianyong Gao – *Walter Schottky Institute and Physics Department, Technical University of Munich, 85748 Garching, Germany*

Peter Müller-Buschbaum – *Chair for Functional Materials, TUM School of Natural Sciences, Technical University of Munich, 85748 Garching, Germany; Heinz Maier-Leibnitz-Zentrum, Technical University of Munich, 85748 Garching, Germany*; orcid.org/0000-0002-9566-6088

Ward van der Stam – *Inorganic Chemistry and Catalysis, Department of Chemistry, Utrecht University, 3584 CG Utrecht, The Netherlands*; orcid.org/0000-0001-8155-5400

Complete contact information is available at: <https://pubs.acs.org/doi/10.1021/acscatal.2c05235>

Notes

The authors declare no competing financial interest.

■ ACKNOWLEDGMENTS

This work received support from the European Research Council (ERC) under the European Union's Horizon 2020 research and innovation programme (grant agreement no. 864234) and from the Deutsche Forschungsgemeinschaft (DFG, German Research Foundation) under Germany's Excellence Strategy – EXC 2089/1 – 390776260 as well as from TUM.solar in the context of the Bavarian Collaborative Research Project Solar Technologies Go Hybrid (SolTech). P.D. and T.G. acknowledge support from China Scholarship Council (CSC). B.M.W. acknowledges funding from the Netherlands Center for Multiscale Catalytic Energy Conversion (MCEC), an NWO Gravitation program funded by the Ministry of Education, Culture and Science of the government of the Netherlands. The authors thank M. Schwartzkopf (Deutsches Elektronen-Synchrotron DESY, Germany) and S.V. Roth (Deutsches Elektronen-Synchrotron DESY, Germany) for their help with setting up the beamline P03 at DESY. GISAXS measurements were carried out at light source PETRA III at DESY, a member of the Helmholtz Association (HFG).

■ REFERENCES

- (1) De Luna, P.; Christopher, H.; Higgins, D.; Jaffer, S. A.; Jaramillo, T. F.; Sargent, E. H. What Would It Take for Renewably Powered Electrosynthesis to Displace Petrochemical Processes? *Science* **2019**, *364*, No. eaav3506.
- (2) Nitopi, S.; Bertheussen, E.; Scott, S. B.; Liu, X.; Engstfeld, A. K.; Horch, S.; Seger, B.; Stephens, I. E. L.; Chan, K.; Hahn, C.; Nørskov, J. K.; Jaramillo, T. F.; Chorkendorff, I. Progress and Perspectives of Electrochemical CO₂ Reduction on Copper in Aqueous Electrolyte. *Chem. Rev.* **2019**, *119*, 7610–7672.
- (3) Han, N.; Ding, P.; He, L.; Li, Y.; Li, Y. Promises of Main Group Metal-Based Nanostructured Materials for Electrochemical CO₂ Reduction to Formate. *Adv. Energy Mater.* **2020**, *10*, No. 1902338.
- (4) Zhang, X.; Wang, Y.; Gu, M.; Wang, M.; Zhang, Z.; Pan, W.; Jiang, Z.; Zheng, H.; Lucero, M.; Wang, H.; Sterbinsky, G. E.; Ma, Q.; Wang, Y.-G.; Feng, Z.; Li, J.; Dai, H.; Liang, Y. Molecular Engineering of Dispersed Nickel Phthalocyanines on Carbon Nanotubes for Selective CO₂ Reduction. *Nat. Energy* **2020**, *5*, 684–692.
- (5) Gong, Q.; Ding, P.; Xu, M.; Zhu, X.; Wang, M.; Deng, J.; Ma, Q.; Han, N.; Zhu, Y.; Lu, J.; Feng, Z.; Li, Y.; Zhou, W.; Li, Y. Structural Defects on Converted Bismuth Oxide Nanotubes Enable Highly Active Electrocatalysis of Carbon Dioxide Reduction. *Nat. Commun.* **2019**, *10*, No. 2807.
- (6) Ding, P.; Zhang, J.; Han, N.; Zhou, Y.; Jia, L.; Li, Y. Simultaneous Power Generation and CO₂ Valorization by Aqueous Al–CO₂ Batteries Using Nanostructured Bi₂S₃ as the Cathode Electrocatalyst. *J. Mater. Chem. A* **2020**, *8*, 12385–12390.
- (7) Yang, H. B.; Hung, S.-F.; Liu, S.; Yuan, K.; Miao, S.; Zhang, L.; Huang, X.; Wang, H.-Y.; Cai, W.; Chen, R.; Gao, J.; Yang, X.; Chen, W.; Huang, Y.; Chen, H. M.; Li, C. M.; Zhang, T.; Liu, B. Atomically Dispersed Ni(I) as the Active Site for Electrochemical CO₂ Reduction. *Nat. Energy* **2018**, *3*, 140–147.
- (8) Birdja, Y. Y.; Pérez-Gallent, E.; Figueiredo, M. C.; Göttle, A. J.; Calle-Vallejo, F.; Koper, M. T. M. Advances and Challenges in Understanding the Electrocatalytic Conversion of Carbon Dioxide to Fuels. *Nat. Energy* **2019**, *4*, 732–745.
- (9) Gauthier, J. A.; Stenlid, J. H.; Abild-Pedersen, F.; Head-Gordon, M.; Bell, A. T. The Role of Roughening to Enhance Selectivity to C₂₊ Products during CO₂ Electroreduction on Copper. *ACS Energy Lett.* **2021**, *6*, 3252–3260.

- (10) Zhu, Q.; Sun, X.; Yang, D.; Ma, J.; Kang, X.; Zheng, L.; Zhang, J.; Wu, Z.; Han, B. Carbon Dioxide Electroreduction to C_2 Products over Copper-Cuprous Oxide Derived from Electrosynthesized Copper Complex. *Nat. Commun.* **2019**, *10*, No. 3851.
- (11) Sun, Z.; Hu, Y.; Zhou, D.; Sun, M.; Wang, S.; Chen, W. Factors Influencing the Performance of Copper-Bearing Catalysts in the CO_2 Reduction System. *ACS Energy Lett.* **2021**, *6*, 3992–4022.
- (12) Chen, X.; Chen, J.; Alghoraibi, N. M.; Henckel, D. A.; Zhang, R.; Nwabara, U. O.; Madsen, K. E.; Kenis, P. J. A.; Zimmerman, S. C.; Gewirth, A. A. Electrochemical CO_2 -to-Ethylene Conversion on Polyamine-Incorporated Cu Electrodes. *Nat. Catal.* **2021**, *4*, 20–27.
- (13) Rossi, K.; Buonsanti, R. Shaping Copper Nanocatalysts to Steer Selectivity in the Electrochemical CO_2 Reduction Reaction. *Acc. Chem. Res.* **2022**, *55*, 629–637.
- (14) Mistry, H.; Varela, A. S.; Köhl, S.; Strasser, P.; Cuenya, B. R. Nanostructured Electrocatalysts with Tunable Activity and Selectivity. *Nat. Rev. Mater.* **2016**, *1*, No. 16009.
- (15) Zhong, M.; Tran, K.; Min, Y.; Wang, C.; Wang, Z.; Dinh, C.-T.; de Luna, P.; Yu, Z.; Rasouli, A. S.; Brodersen, P.; Sun, S.; Voznyy, O.; Tan, C.-S.; Askerka, M.; Che, F.; Liu, M.; Seifitokaldani, A.; Pang, Y.; Lo, S.-C.; Ip, A.; Ulissi, Z.; Sargent, E. H. Accelerated Discovery of CO_2 Electrocatalysts Using Active Machine Learning. *Nature* **2020**, *581*, 178–183.
- (16) Lee, C. W.; Yang, K. D.; Nam, D.-H.; Jang, J. H.; Cho, N. H.; Im, S. W.; Nam, K. T. Defining a Materials Database for the Design of Copper Binary Alloy Catalysts for Electrochemical CO_2 Conversion. *Adv. Mater.* **2018**, *30*, No. 1704717.
- (17) Xu, A.; Govindarajan, N.; Kastlunger, G.; Vijay, S.; Chan, K. Theories for Electrolyte Effects in CO_2 Electroreduction. *Acc. Chem. Res.* **2022**, *55*, 495–503.
- (18) Huang, J. E.; Li, F.; Ozden, A.; Rasouli, A. S.; de Arquer, F. P. G.; Liu, S.; Zhang, S.; Luo, M.; Wang, X.; Lum, Y.; Xu, Y.; Bertens, K.; Miao, R. K.; Dinh, C.-T.; Sinton, D.; Sargent, E. H. CO_2 electrolysis to multicarbon products in strong acid. *Science* **2021**, *372*, 1074–1078.
- (19) Zhang, X.; Li, J.; Li, Y.-Y.; Jung, Y.; Kuang, Y.; Zhu, G.; Liang, Y.; Dai, H. Selective and High Current CO_2 Electro-Reduction to Multicarbon Products in Near-Neutral KCl Electrolytes. *J. Am. Chem. Soc.* **2021**, *143*, 3245–3255.
- (20) Burdyny, T.; Smith, W. A. CO_2 Reduction on Gas-Diffusion Electrodes and Why Catalytic Performance Must Be Assessed at Commercially-Relevant Conditions. *Energy Environ. Sci.* **2019**, *12*, 1442–1453.
- (21) Pham, T. H. M.; Zhang, J.; Li, M.; Shen, T.-H.; Ko, Y.; Tileli, V.; Luo, W.; Züttel, A. Enhanced Electrocatalytic CO_2 Reduction to C_{2+} Products by Adjusting the Local Reaction Environment with Polymer Binders. *Adv. Energy Mater.* **2022**, *12*, No. 2103663.
- (22) Chang, Q.; Lee, J. H.; Liu, Y.; Xie, Z.; Hwang, S.; Marinkovic, N. S.; Park, A.-H. A.; Kattel, S.; Chen, J. G. Electrochemical CO_2 Reduction Reaction over Cu Nanoparticles with Tunable Activity and Selectivity Mediated by Functional Groups in Polymeric Binder. *JACS Au* **2022**, *2*, 214–222.
- (23) Kim, C.; Bui, J. C.; Luo, X.; Cooper, J. K.; Kusoglu, A.; Weber, A. Z.; Bell, A. T. Tailored Catalyst Microenvironments for CO_2 Electroreduction to Multicarbon Products on Copper Using Bilayer Ionomer Coatings. *Nat. Energy* **2021**, *6*, 1026–1034.
- (24) Kusoglu, A.; Weber, A. Z. New Insights into Perfluorinated Sulfonic-Acid Ionomers. *Chem. Rev.* **2017**, *117*, 987–1104.
- (25) Li, G.-F.; Yang, D.; Chuang, P.-Y. A. Defining Nafion Ionomer Roles for Enhancing Alkaline Oxygen Evolution Electrocatalysis. *ACS Catal.* **2018**, *8*, 11688–11698.
- (26) Tan, Y. C.; Lee, K. B.; Song, H.; Oh, J. Modulating Local CO_2 Concentration as a General Strategy for Enhancing C–C Coupling in CO_2 Electroreduction. *Joule* **2020**, *4*, 1104–1120.
- (27) Berlinger, S. A.; McCloskey, B. D.; Weber, A. Z. Inherent Acidity of Perfluorosulfonic Acid Ionomer Dispersions and Implications for Ink Aggregation. *J. Phys. Chem. B* **2018**, *122*, 7790–7796.
- (28) Berlinger, S. A.; Duden, P. J.; Bird, A.; Chen, X.; Freychet, G.; McCloskey, B. D.; Kusoglu, A.; Weber, A. Z. Impact of Dispersion Solvent on Ionomer Thin Films and Membranes. *ACS Appl. Polym. Mater.* **2020**, *2*, 5824–5834.
- (29) Tarokh, A.; Karan, K.; Ponnuram, S. Atomistic MD Study of Nafion Dispersions: Role of Solvent and Counterion in the Aggregate Structure, Ionic Clustering, and Acid Dissociation. *Macromolecules* **2020**, *53*, 288–301.
- (30) de Arquer, F. P. G.; Dinh, C. T.; Ozden, A.; Wicks, J.; McCallum, C.; Kirmani, A. R.; Nam, D. H.; Gabardo, C.; Seifitokaldani, A.; Wang, X.; Li, Y. C.; Li, F. W.; Edwards, J.; Richter, L. J.; Thorpe, S. J.; Sinton, D.; Sargent, E. H. CO_2 electrolysis to multicarbon products at activities greater than 1 A cm^{-2} . *Science* **2020**, *367*, 661–666.
- (31) Li, T. Is More CO_2 Beneficial for Making Multi-Carbon Products? *Joule* **2020**, *4*, 980–982.
- (32) Gao, X.; Yamamoto, K.; Hirai, T.; Ohta, N.; Uchiyama, T.; Watanabe, T.; Imai, H.; Sugawara, S.; Shinohara, K.; Uchimoto, Y. Impact of the Composition of Alcohol/Water Dispersion on the Proton Transport and Morphology of Cast Perfluorinated Sulfonic Acid Ionomer Thin Films. *ACS Omega* **2021**, *6*, 14130–14137.
- (33) Lum, Y.; Ager, J. W. Evidence for Product-Specific Active Sites on Oxide-Derived Cu Catalysts for Electrochemical CO_2 Reduction. *Nat. Catal.* **2019**, *2*, 86–93.
- (34) Lum, Y.; Yue, B.; Lobaccaro, P.; Bell, A. T.; Ager, J. W. Optimizing C–C Coupling on Oxide-Derived Copper Catalysts for Electrochemical CO_2 Reduction. *J. Phys. Chem. C* **2017**, *121*, 14191–14203.
- (35) Lum, Y.; Ager, J. W. Stability of Residual Oxides in Oxide-Derived Copper Catalysts for Electrochemical CO_2 Reduction Investigated with ^{18}O Labeling. *Angew. Chem., Int. Ed.* **2018**, *57*, 551–554.
- (36) de Yuso, M. V. M.; Neves, L. A.; Coelho, I. M.; Crespo, J. G.; Benavente, J.; Rodríguez-Castellón, E. A study of chemical modifications of a Nafion membrane by incorporation of different room temperature ionic liquids. *Fuel Cells* **2012**, *12*, 606–613.
- (37) Wang, S.; Kou, T.; Baker, S. E.; Duoss, E. B.; Li, Y. Recent Progress in Electrochemical Reduction of CO_2 by Oxide-Derived Copper Catalysts. *Mater. Today Nano* **2020**, *12*, No. 100096.
- (38) Bui, J. C.; Kim, C.; King, A. J.; Romiluyi, O.; Kusoglu, A.; Weber, A. Z.; Bell, A. T. Engineering Catalyst–Electrolyte Microenvironments to Optimize the Activity and Selectivity for the Electrochemical Reduction of CO_2 on Cu and Ag. *Acc. Chem. Res.* **2022**, *55*, 484–494.
- (39) de Gregorio, G. L.; Burdyny, T.; Loiudice, A.; Iyengar, P.; Smith, W. A.; Buonsanti, R. Facet-Dependent Selectivity of Cu Catalysts in Electrochemical CO_2 Reduction at Commercially Viable Current Densities. *ACS Catal.* **2020**, *10*, 4854–4862.
- (40) Luo, W.; Nie, X.; Janik, M. J.; Asthagiri, A. Facet Dependence of CO_2 Reduction Paths on Cu Electrodes. *ACS Catal.* **2016**, *6*, 219–229.
- (41) Grosse, P.; Yoon, A.; Rettenmaier, C.; Herzog, A.; Chee, S. W.; Cuenya, B. R. Dynamic Transformation of Cubic Copper Catalysts during CO_2 Electroreduction and Its Impact on Catalytic Selectivity. *Nat. Commun.* **2021**, *12*, No. 6736.
- (42) Zhan, C.; Dattila, F.; Rettenmaier, C.; Bergmann, A.; Köhl, S.; García-Muelas, R.; López, N.; Cuenya, B. R. Revealing the CO Coverage-Driven C–C Coupling Mechanism for Electrochemical CO_2 Reduction on Cu_2O Nanocubes via Operando Raman Spectroscopy. *ACS Catal.* **2021**, *11*, 7694–7701.
- (43) Jiang, S.; Klingan, K.; Pasquini, C.; Dau, H. New Aspects of Operando Raman Spectroscopy Applied to Electrochemical CO_2 Reduction on Cu Foams. *J. Chem. Phys.* **2018**, *150*, No. 041718.
- (44) Moradzaman, M.; Mul, G. In Situ Raman Study of Potential-Dependent Surface Adsorbed Carbonate, CO, OH, and C Species on Cu Electrodes During Electrochemical Reduction of CO_2 . *ChemElectroChem* **2021**, *8*, 1478–1485.
- (45) de Ruiter, J.; An, H.; Wu, L.; Gijsberg, Z.; Yang, S.; Hartman, T.; Weckhuysen, B. M.; van der Stam, W. Probing the Dynamics of

Low-Overpotential CO₂-to-CO Activation on Copper Electrodes with Time-Resolved Raman Spectroscopy. *J. Am. Chem. Soc.* **2022**, *144*, 15047–15058.

(46) An, H.; Wu, L.; Mandemaker, L. D. B.; Yang, S.; de Ruiter, J.; Wijten, J. H. J.; Janssens, J. C. L.; Hartman, T.; van der Stam, W.; Weckhuysen, B. M. Sub-Second Time-Resolved Surface-Enhanced Raman Spectroscopy Reveals Dynamic CO Intermediates during Electrochemical CO₂ Reduction on Copper. *Angew. Chem., Int. Ed.* **2021**, *60*, 16576–16584.

(47) Zhao, Y.; Chang, X.; Malkani, A. S.; Yang, X.; Thompson, L.; Jiao, F.; Xu, B. Speciation of Cu Surfaces During the Electrochemical CO Reduction Reaction. *J. Am. Chem. Soc.* **2020**, *142*, 9735–9743.

(48) Niaura, G. Surface-Enhanced Raman Spectroscopic Observation of Two Kinds of Adsorbed OH[−] Ions at Copper Electrode. *Electrochim. Acta* **2000**, *45*, 3507–3519.

(49) Gao, J.; Zhang, H.; Guo, X.; Luo, J.; Zakeeruddin, S. M.; Ren, D.; Grätzel, M. Selective C–C Coupling in Carbon Dioxide Electroreduction via Efficient Spillover of Intermediates as Supported by Operando Raman Spectroscopy. *J. Am. Chem. Soc.* **2019**, *141*, 18704–18714.

Recommended by ACS

Mitigating Electrode Inactivation during CO₂ Electrocatalysis in Aprotic Solvents with Alkali Cations

Benjamin C. Kash, Chibueze V. Amanchukwu, *et al.*

JANUARY 20, 2023

THE JOURNAL OF PHYSICAL CHEMISTRY LETTERS

READ 

Product Distribution Control Guided by a Microkinetic Analysis for CO Reduction at High-Flux Electrocatalysis Using Gas-Diffusion Cu Electrodes

Xiaofei Lu, Kazuhiro Takanabe, *et al.*

JANUARY 17, 2023

ACS CATALYSIS

READ 

Localized Alkaline Environment via In Situ Electrostatic Confinement for Enhanced CO₂-to-Ethylene Conversion in Neutral Medium

Zihong Wang, Xiaodi Ren, *et al.*

MARCH 09, 2023

JOURNAL OF THE AMERICAN CHEMICAL SOCIETY

READ 

Quantitative Understanding of Cation Effects on the Electrochemical Reduction of CO₂ and H⁺ in Acidic Solution

Hai-Gang Qin, Jun Gu, *et al.*

DECEMBER 29, 2022

ACS CATALYSIS

READ 

Get More Suggestions >